Real-time in situ magnetic measurement of the intracellular biodegradation of iron oxide nanoparticles in a stem cell-spheroid tissue model

Aurore van de Walle, Alexandre Fromain, Anouchka Plan Sangnier, Alberto Curcio, Luc Lenglet, Laurence Motte, Yoann Lalatonne, Claire Wilhelm

Real-time in situ magnetic measurement of the intracellular biodegradation of iron oxide nanoparticles in a stem cell-spheroid tissue model

Aurore Van de Walle[1*], Alexandre Fromain[1], Anouchka Plan Sangnier[1,2], Alberto Curcio[1], Luc Lenglet[3], Laurence Motte[2], Yoann Lalatonne[2,4*], Claire Wilhelm[1*]

[1] Laboratoire Matière et Systèmes, Complexes MSC, UMR 7057, CNRS & University Paris Diderot, 75205, Paris Cedex 13, France
[2] Inserm, U1148, Laboratory for Vascular Translational Science, Université Paris 13, Sorbonne Paris Cité, F-93017 Bobigny, France
[3] Normafin Sàrl, 8 rue Mathilde Girault, 92300 Levallois-Perret

[4] Services de Biochimie et Médecine Nucléaire, Hôpital Avicenne Assistance Publique-Hôpitaux de Paris F-93009 Bobigny, France.
**send correspondence to* Aurore Van de Walle, aurore.vandewalle@univ-paris-diderot.fr; Yoann Lalatonne, yoann.lalatonne@aphp.fr; Claire Wilhelm, claire.wilhelm@univ-paris-diderot.fr

Abstract

The use of magnetic nanoparticles in nanomedicine keeps expending and, for most applications, the nanoparticles are internalized in cells then left within, bringing the need for accurate, fast, and easy to handle methodologies to assess their behavior in the cellular environment. Herein, a benchtop-size magnetic sensor is introduced to provide real-time precise measurement of nanoparticle magnetism within living cells. The values obtained with the sensor, of cells loaded with different doses of magnetic nanoparticles, are first compared to conventional vibrating sample magnetometry (VSM), and a strong correlation remarkably validates the use of the magnetic sensor as magnetometer to determine the nanoparticle cellular uptake. The sensor is then used to monitor the progressive intracellular degradation of the nanoparticles, over days. Importantly, this real-time *in situ* measure is performed on a stem cell-spheroid tissue model and can run continuously on a same spheroid, with cells kept alive within. Besides, such continuous magnetic measurement of cell magnetism at the tissue scale does not impact either tissue formation, viability, or stem cell function, including differentiation and extracellular matrix production.

Keywords: magnetic nanoparticles, magnetometry, real-time in operando measures, biodegradation, stem cells.

Introduction

Magnetic nanoparticles provide extended feature for a vast range of biomedical applications. They were first developed as magnetic resonance imaging (MRI) contrast agents [1–4], for some already at disposition in the clinic [5]. They have since been developed as cancer treatment agent, for killing diseased cells via magnetic hyperthermal [3,4,6–15] or photothermal [9,16–19] procedures, and as carriers for drug delivery [10,12,20–23]. More recently, their use has been implemented in tissue regeneration [24–26], for cell guidance at a distance and the possibility of creating cellular tissues whose fate upon implantation can be monitored by MRI [27]. In this context, the nanoparticles' integration within the body and progressive clearance from it have been extensively studied. Along their circulation in the bloodstream they are first captured mainly by the macrophages of the liver (Kupffer cells), spleen, and bone marrow, where iron content peaks within hours and are then progressively degraded [28–32]. These *in vivo* results provide a general understanding about how nanoparticles behave in the body. Nonetheless, precise quantitative monitoring of their degradation at the heart of cells is still an open challenge. Some *in vitro* studies completed the initial *in vivo* observations by assessing the fate of the nanoparticles upon internalization within cells, on fixed cells, at given time points [33–35]. They confirmed that, upon incorporation within cells, magnetic nanoparticles are progressively degraded over the course of a month. For these studies, the cell samples harvested at different time intervals were analyzed by conventional magnetometry measurements (e.g. vibrating sample magnetometry (VSM), superconducting quantum interference device (SQUID)) and correlated with total iron quantifications, obtained via inductively coupled plasma mass spectrometry (ICP-MS) [33–35]. The magnetometry signal is then considered as a direct representation of the integrity of the nanoparticles: when the magnetic signal decreases while total iron remains constant, it is the signature of the nanoparticle degradation [33]. Despite bringing additional knowledge on the nanoparticle fate, these methods do not allow real-time analyses due to the impossibility of keeping cells viable along the experiments. Results are thus obtained on discrete samples and, as such, due to the multitude of samples needed, are either performed once a day on a short time period, or every few days or even weeks when on a longer time frame. Oppositely, probing properties at the nanoparticle level in real-time is important for monitoring their structure upon their potential degradation, or over their therapeutic action (in operando). Such systems are being developed and the impact of magnetic nanoparticles heating on a thermosensitive surface coating has for example been monitored upon real-time magnetic hyperthermia application [36].

Standard magnetometry methods require the use of specific equipment that are often large scale and not readily available. Consequently, analysis of cell labeling efficiency on living cells right upon labeling is usually impossible. This remains an important limitation for any further biomedical application as nanoparticle type (core structure [37] and coating [38]), concentration, incubation time but also cell type [38] and donor [39] clearly influence the internalization rate. As a consequence, variations in labeling efficiency are not evaluated even though a tightly regulated "dose" of nanoparticles per cell is required as it might otherwise affect cellular functionality. Indeed, it has been shown that a high dose of nanoparticles can inhibit mesenchymal stem cell differentiation and even lead to cellular apoptosis [40–44].

A solution for a fast and effective quantification of nanoparticles' internalization within cells can be provided by a benchtop magnetic device first developed by Nikitin et al. and further explored for applications ranging from electrical engineering to life science [45,46]. The physical concept is to expose the superparamagnetic nanoparticles to a two-frequency magnetic field and the resulting nonlinear magnetization of the nanoparticles generates a response signal which is strictly proportional to the quantities of magnetic nanoparticles.

Herein, thanks to this magnetic sensor system, we managed not only to quantify in real-time the internalization of magnetic nanoparticles within human stem cells, but also and to monitor their integrity over days in a stem cells-derived spheroid-like tissue model [33–35], without impacting stem cells viability and differentiation capacity. It is a consequent advance compared to previous works where the use of conventional magnetometry precluded any measurement on living cells, and allowed thus only discrete evaluation at time intervals very distant considering the kinetics of the degradation process, also precluding the use of the same sample, with the risk of introducing biological variability. Besides being a technical challenge, such measurement of magnetic nanoparticles integrity in operando (in real time, in situ, on living cells, and upon degradation) could become a unique companion test to non-invasively characterize magnetically engineered tissues prior to implantation for regenerative medicine.

1. Material and Methods

1.1.Magnetic Nanoparticles' synthesis

Magnetic nanoparticles were synthesized as previously described [47]. Briefly, 400 mg of iron(III) acetylacetonate (> 99.9%) (Sigma Aldrich) were dissolved in 10 ml of benzyl alcohol anhydrous (99.8%) (Sigma Aldrich). This solution was placed in a Monowave 300 from Anton Paar and the temperature of the suspension was increased up to 250°C in 20 minutes then

maintained constant for 30 minutes. The resulting suspension was precipitated using a neodymium magnet and washed successively with dichloromethane, sodium hydroxyde, ethanol, and water (pH=7). A last washing step was performed in acidic water (pH=2) and the nanoparticles were separated by ultracentrifugation using an Amicon® ultra centrifugal filters (30 kD). Finally, the magnetic nanoparticles were resuspended in acidic water (pH=2) for further coating.

1.2.Magnetic nanoparticles' coating

Citric acid (from Sigma Aldrich) and polyethylene glycol (PEG) phosphonic carboxylic acid (from Specific Polymers, SP-1P-10-002, MW 2500 g mol^{-1}) were dissolved in water at pH=2. Coating must be in excess with mass ratio 5-times higher than nanoparticles. The coating molecule solution and nanoparticle dispersion were mixed and left for 2 hours under magnetic stirring. At the end of the reaction, pH was adjusted at 7, and the system is left to equilibrate for 2 hours. Finally, nanoparticles were magnetically purified 3 times in water (pH=2) then ultra-centrifuged at pH=7 in Amicon® ultra centrifugal filters (30 kD). The two coatings are named in the following citrate and PEG.

1.3.Cell culture and nanoparticles' internalization

Human mesenchymal stem cells (Lonza) were cultured in MSCBM medium (Lonza) with the provided kit containing serum, glutamine and antibiotics, at 37°C with 5% CO_2. Cells were amplified until passage 4-5 then were allowed to grow until near confluence prior to labelling. Cells were washed first with RPMI then incubated with the labelling solution for 24 hours for PEG coating and for 30 minutes for citrate coating due to their faster internalization rate provided by the negative surface charge [34]. The labelling solution was composed of nanoparticles dispersed in serum-free RPMI-1640 medium (ThermoFischer Scientific) at iron concentrations between 0.1 and 4 mM. In the case of the experiments performed on citrate-coated nanoparticles in real-time, the media was supplemented with 5mM sodium citrate. Upon labelling, cells were rinsed with RPMI then media was replaced by MSCBM medium for 1 hour to allow a complete internalization of the nanoparticles before further processing **(Fig. 1A)**.

1.4.Cell spheroids' formation and culture

Cells loaded with nanoparticles were detached with Trypsin-EDTA (0.05%) phenol red (thermoFisher Scientifc), then 200 000 cells were dispersed in 1.5 ml of medium in 15 ml Falcon® tubes before being centrifuged for 5 minutes at 120 g to form a high-density pellet.

Pellets remained in culture at 37 °C and 5% CO_2 in medium composed of DMEM high glucose supplemented with 1% penicillin streptomycin, 1% ITS premix (Corning), with final concentrations of: 0.1 µM of dexamethasone (Sigma), 1 mM sodium pyruvate (Sigma), 50 µM ascorbic acid-2 phosphate (Sigma) and 0.35 mM L-proline (Sigma). The media was replenished twice a week. To induce extracellular matrix production, the growth factor TGF-β3 (10 ng/ml) was added to the culture medium.

For magnetometry analyses of discrete samples, spheroids were washed with cacodylate buffer (0.1 M) then fixed with a solution of 2% glutaraldehyde in 0.1 M cacodylate buffer for 30 minutes at room temperature and stored in PBS in order to measure their macroscopic magnetization at different days of the maturation process (days 1, 4, 8, and 21).

For real-time magnetometry analyses, the same sample remained in culture along the measurements with the magnetic sensor. The impact of real-time measurements on cell viability was also assessed by studying if it had an effect on cell function and associated tissue formation. To do so, stem cell spheroids cultured in medium supplemented with the growth factor TGF-β3 were continuously kept in the magnetic sensor for 6 days, time during which tissue formation is initiated, and were then kept in standard incubator for 15 extra days, to allow further extracellular matrix production. This extracellular matrix production was then observed with TEM and histology, quantified via PCR, and compared to control spheroids cultured in incubator only.

1.5.Magnetometry measurements using the magnetic sensor

The magnetic sensor was developed by Magnisense SA for diagnostic tests. Here it was used to quantify the iron oxide nanoparticles in the cellular environment (see photograph in Fig. S1A). The analysis is based on the non-linear superparamagnetic magnetization of thenanoparticles [48]. Briefly, an alternating magnetic field is applied to the sample at two different frequencies f_1 = 100 kHz and f_2 = 100 Hz of different amplitudes 10 and 200 Oe, respectively. The signal measured represents the third derivative of the sample magnetization at zero magnetic field and room temperature, proportional to the amount of nanoparticles within the sample.

For real-time measurement of cell spheroids magnetization, a 5% CO_2 environment was achieved via direct injection of 5% CO_2 into a home-made bioreactor. Temperature was adjusted such as the final temperature within the sensor remained at 37°C. Control samples were kept in standard incubator, at 5% CO_2 and 37°C.

1.6.Measurements via Vibrating Sample Magnetometry (VSM)

As a comparison to the magnetic sensor signal, samples were analysed by VSM (Quantum Design, Versalab; see photograph in Fig. S1B) that directly provides the magnetic moment (expressed in emu) of a sample when submitted to a magnetic field. The spheroids composed of 200 000 cells were introduced in the VSM. Field-dependent magnetization curves were recorded as a function of the applied filed between 0 and 25 000 Oe and provide magnetization at saturation.

1.7.Histological analyses

After 21 days of culture, cell aggregates were washed twice with PBS before being fixed in 4% paraformaldehyde. Samples were then embedded in OCT (Optimal Cutting Temperature) compound, frozen using isopentane cooled in a liquid nitrogen bath, and cryosectionned (8 µm-thick slices). The slices were stained with Fast green and Safranin O (0.1%) to reveal the presence of extracellular matrix components (glycosaminoglycans).

1.8.Transmission electron microscopy (TEM) imaging

For TEM imaging, cells labelled with citrate nanoparticles were harvested at days 1 and 21. Samples were rinsed and fixed using 2% glutaraldehyde in 0.1 M cacodylate buffer (Sigma). Samples were then contrasted with oolong tea extract (OTE) 0.5% in cacodylate buffer, post fixed with 1% osmium tetroxide containing 1.5% potassium cyanoferrate then dehydrated in graded ethanol baths and embedded in Epon resin. Ultrathin sections (70 nm) were deposited onto 200 mesh cooper grids and examined (Mima2 INRA platform) with a Hitachi HT 7700 TEM operated at 80 kV with image acquisition using a charge-coupled device camera (AMT).

1.9.Relative quantification of gene expression by quantitative RT-PCR

Total RNA was extracted from spheroids of the magnetic sensor and of the incubator conditions (for these two conditions the spheroids were cultured with growth factors, to drive extracellular matrix production and tissue formation) using the total RNA isolation kit (Machery-Nagel). The synthesis of complementary DNA (cDNA) was then achieved using SuperScript II Reverse Transcriptase (Invitrogen). Real-time quantitative polymerase chain reaction was performed using the SYBRGreen dye (Applied Biosystems) and conducted with the StepOnePlus detection system (Thermo Fisher Scientific), according to the manufacturer's protocol. The specificity of the reaction was confirmed by melting curves analysis and the fluorescence cycle threshold (Ct) value of each mRNA was obtained. Relative expression of each gene was

performed using the comparative Ct method. First, levels of genes of interest (I) mRNA were normalized to the housekeeping gene ribosomal protein large subunit P0 (RPLP0) ($\Delta Ct = Ct_I - Ct_{RPLP0}$). The relative amount of mRNA levels between the conditions assessed (magnetic sensor or incubator) and the control (spheroids cultured without growth factors in the standard incubator) is then given by $2^{-\Delta\Delta Ct}$, where $\Delta\Delta Ct = [\Delta Ct_I \text{ condition assessed}] - [\Delta Ct_I \text{ control}]$. See Table S1 for primer sequences.

2. Results

2.1.Magnetic quantification of nanoparticles internalization and degradation in stem cells spheroids with both VSM magnetometry and magnetic sensor (discrete assessments)

Human stem cells were incubated with varying iron concentrations (0.5, 1, 2 and 4 mM) of the magnetic nanoparticles (**Fig. 1A**). A total of 200 000 stem cells were then pooled and centrifuged into forming a spheroid which could be kept in culture for up to 21 days in conditions that promote 3D tissue formation (Fig. 1A) [35]. Importantly, in this specific spheroid model, the stem cells stop dividing as soon as they are confined in 3D and start differentiating. As a consequence, no tissue necrosis is detected, over the whole process of spheroid tissue maturation, up to the three weeks of culture, as observed on hematoxylin and eosin staining shown in Fig. S?. For discrete magnetic measurements, spheroid samples were collected at days 1, 4, 8, and 21 ($n \geq 3$ for each day), fixed, and magnetism was analyzed via both the magnetic sensor and the VSM as a standard measurement approach (Fig. 1B). These discrete measurements require the use of multiple samples for the follow-up of the cell magnetism over days, contrasting with continuous measurements on a same spheroid if the samples were kept alive (Fig. 1C). With VSM magnetometry, the magnetic moment of the spheroid sample is directly measured at varying magnetic field, providing both the magnetic susceptibility and the saturation magnetization, directly proportional to the amount of intact nanoparticles in the sample. By contrast, the magnetic sensor measure consists in recording the sample response to an alternating magnetic field created by the sum of two distinct frequency signal, at f_1 = 100 kHz and f_2 = 100 Hz and with different amplitudes of 10 and 200 Oe, respectively. The magnetic response of the sample has then a characteristic shape, which flattens at the extrema, due to the non-linear magnetization of superparamagnetic nanoparticles (Fig. 1D and 1E). By performing the Fourier transform of this signal, the response of the sample at combinatorial frequencies $f = f_1 \pm 2\, f_2$ can be determined and the third derivative of this value is the output signal of the magnetic sensor that we here express in arbitrary units (Fig. 1F). This

signal is directly proportional to the quantity of magnetic material in the sample and the detection threshold is within nanograms for iron oxide nanoparticles of a given size range.

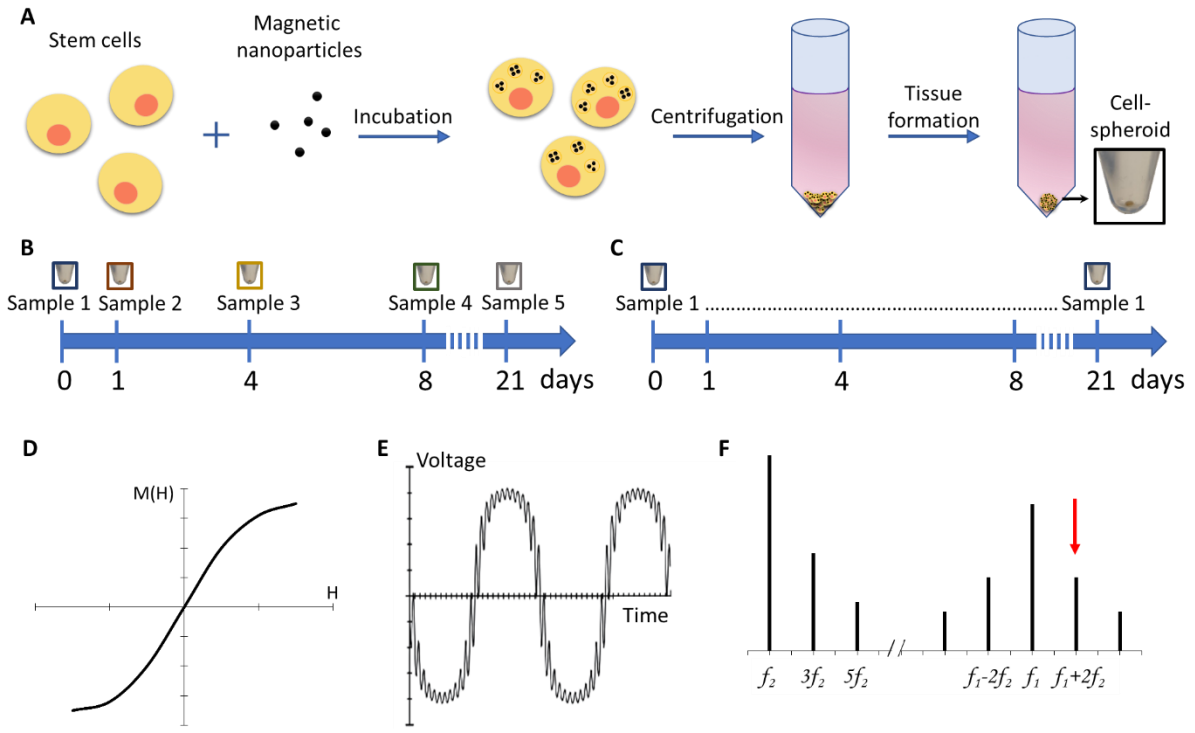

Figure 1: Experimental set-up. A) Stem cells are incubated with magnetic nanoparticles and, upon internalization, the cells are centrifuged to form cohesive 3D spheroids. B) Standard assessments of the integrity of magnetic nanoparticles in cells require the use of multiple independent samples due to the need of fixing them. C) With the magnetic sensor, the cell spheroids can be kept viable and measurements can be performed on a same sample over long time-frames. D) Typical non-linear magnetization curve of superparamagnetic nanoparticles showing the magnetic moment that flattens at high and low magnetic fields. E) Time-dependent voltage of the samples when subjected to the two-frequency magnetic field in the magnetic sensor, this response signal flattens at the extrema due to the non-linear magnetization of the nanoparticles. F) Specific combinatory frequencies in the Fourier-transformed response signal are proportional to the amount of magnetic nanoparticles (red arrow).

Fig. 2A-D presents all measurements obtained at different times of the spheroids' maturation. The VSM measurements (**Fig. 2A-B**) provide the magnetic moments of the samples, expressed

in emu while the magnetic sensor values represent the magnetic signal measured by the sensor (**Fig. 2C-D**). The VSM data showed in **Fig. 2A-B** provide first the internalized dose of the nanoparticles (at day 1), these emu values can be converted into the number of internalized nanoparticles (a 9-nm nanoparticle has a magnetic moment at saturation of 10^{-16} emu), as depicted on the secondary vertical axis in the VSM graphs (**Fig. 2A-B**). These values correspond to 200 000 cells organized as a spheroid, providing therefore the mean number of nanoparticles within each cell, and revealing a nanoparticle internalization increasing with the incubation dose for both the citrate **(Fig. 2A)** and the PEG coating **(Fig. 2B)**. Values are in the range of millions of nanoparticles per cell, 0.8, 1.3 and 4 million per cell for the citrate-coated nanoparticles incubated at [Fe]=0.5, 1 and 2 mM, respectively; and 2.2, 3.5 and 6.1 million per cell for the PEG-coated nanoparticles incubated at [Fe]=1, 2 and 4 mM, respectively. Following internalization, a progressive decrease in magnetism is observed over the 21 days of tissue culture, reflecting a decrease in the number of still intact nanoparticles within the tissue. Remarkably, the evolution of the magnetic sensor values upon nanoparticles degradation, shown in Fig. 2C-D, is highly similar to the VSM measurements. Besides, and importantly, the total iron content within the spheroids was measured by elemental analysis (Fig. S?), and was found constant of the 21 days of tissue culture, enabling to discard any possibility of cell death and subsequent iron release from the spheroids. Representative TEM images of the cells right after nanoparticle incubation (day 1) show all nanoparticles, about 9 nm in diameter, internalized within the endosomes of the cells **(Fig. 2E-F & S2A)**. After 21 days of culture, the apparition of ~6 nm dots, lighter than the initial nanoparticles, can be observed both within the endosomes and outside, dispersed in the cytoplasm of the cells **(Fig. 2G-H & S2B)**. These dots are representative of iron stored within the ferritin protein and can be correlated with the degradation of the nanoparticles and the consequent release of free iron.

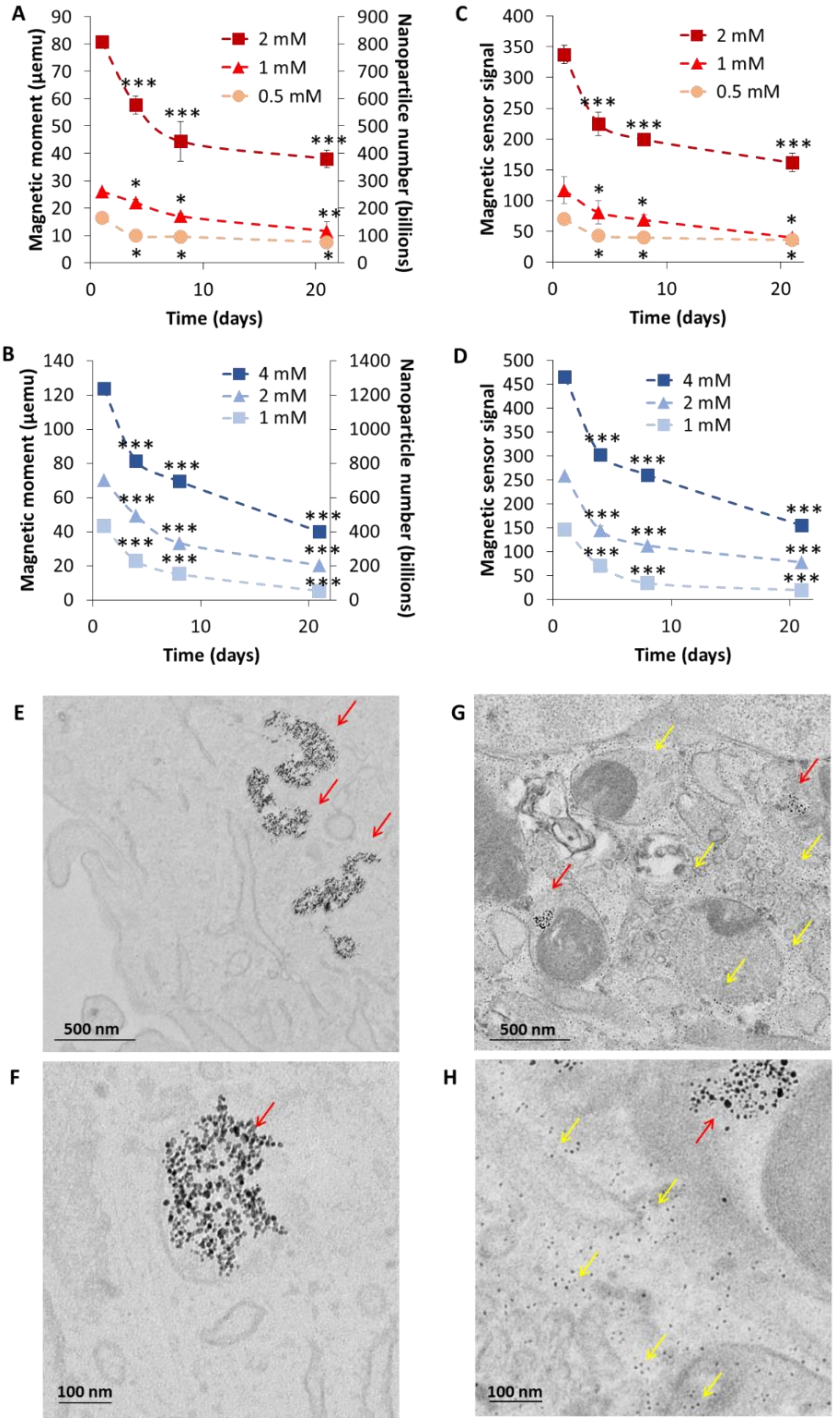

Figure 2: Progressive degradation of magnetic nanoparticles in a stem cell spheroid model similarly quantified via both magnetic sensor and VSM magnetometry techniques. A,B) VSM magnetometry of the stem cells spheroids is performed at days 1, 4, 8, and 21. The saturation magnetic moments of the samples, expressed in µemu can be converted into a number of intact nanoparticles (1µemu equals 10 billion of 9 nm – diameter nanoparticles). Measurements are obtained for three different incubation concentrations and two coatings: A) a citrate and B) a PEG coating. C,D) Similar measurements on the same spheroids, with the magnetic sensor, expressed in the measurement unit of the device. Asterisks indicate significant

differences when compared to day 0, *p<0.05, **p<0.05, ***p<0.001. E, F). Representative TEM images of the cells at day 1 (E,F) and day 21 (G,H). At day 1 (E,F), dark dots can be observed, representative of the nanoparticles that are initially internalized in the endosomes of the cells. At day 21 (G,H), light grey dots appear in the endosomes and the cytoplasm, ranging in the size of the storage ferritin protein loaded with iron. Remaining intact nanoparticles (dark dots) can also be observed in the endosomes. Red arrows: intact nanoparticles, yellow arrows: ferritin proteins.

2.2.A strong correlation between the magnetic sensor signal of intracellular nanoparticles and their VSM magnetic moment

All magnetic sensor values obtained on cellular samples are compared with the VSM measurements in **Fig. 3**, evidencing a strong correlation between the two techniques, with $R^2 > 0.99$, within a very large range of concentrations. The magnetic sensor signal can thus be equaled to a magnetic moment, expressed in emu. However, it has to be kept in mind that the signal obtained with the magnetic sensor depends on the size of the nanoparticles, and such correlation must be determined for each nanoparticle design. Importantly, herein the correlation remains unchanged between day 1 (first day of the nanoparticles within the cells) and at the following days (3 to 21), for samples where a proportion of nanoparticles are already degraded. It indicates that only intact (9 nm in diameter) nanoparticles are measured, meaning that the nanoparticles are either still intact or fully degraded, thus not contributing neither to the VSM signal, nor the magnetic sensor one.

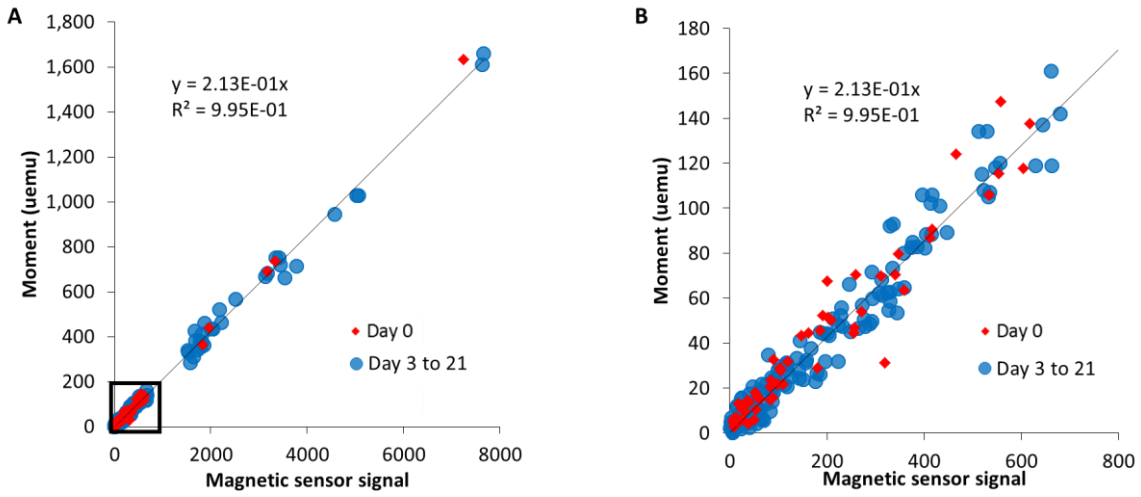

Figure 3: Correlation between the magnetic sensor signal and the magnetic moment obtained via VSM. A-B) A strong correlation is observed between the magnetic sensor and the

VSM measurements of 9 nm iron oxide nanoparticles coated with citrate or PEG, internalized in stem cells and cultured for up to 21 days as cellular spheroids. A) shows the correlation for the entire set of data and B) is a close-up on the lower values (corresponding to the black square of A).

2.3.Real-time in situ follow-up of the nanoparticles degradation in the stem cells spheroids

To investigate the potential of the magnetic sensor to monitor nanoparticle biodegradation in situ within living cells, on the exact same spheroid, independent spheroids were first placed in a traditional incubator and measured once a day using the magnetic sensor. The aim was to observe if repeated punctual measurements of live cells spheroids could be achieved. Two intracellular doses of nanoparticles were chosen: a mild dose of 4-6 million nanoparticles per cell, dose achieved for the nanoparticles with the citrate coating; and a low dose of 1-2 million nanoparticles per cell, achieved with the PEG-coated nanoparticles, to test the limits of the sensor. Results are shown in **Fig. 4A** and **Fig. 4D**, for citrate-coated and PEG-coated nanoparticles, respectively, and clearly demonstrate that the measurements are reliable, as shown by the progressive decrease in the magnetic sensor signal, the excellent reproducibility amongst the spheroids, and a similar degradation profile than the one obtained on fixed samples. Then, a home-made incubator was specifically adapted to the magnetic sensor, designed to mimic the culture conditions encountered in a traditional incubator, with 5% CO_2 and 37˚C temperature (Fig. S3). Using this set-up, continuous measurements were obtained on single spheroids for 6 days in a raw, with data taken every 0.5 seconds then averaged every 10 minutes. Typical curves of the resulting magnetic signal are shown in **Fig. 4B-4C** and **Fig 4E-4F**, for citrate-coated and PEG-coated nanoparticles, respectively, and a progressive decrease in the signal is evidenced for all spheroids assessed, similarly to the data previously observed on punctual assessments **(Figs. 4A** and **4D)**. Besides, **Figs. 4B** and **4E** correspond to single spheroid prepared and investigated at the same time as the ones measured punctually in **Figs. 4A** and **4D**. Instead of obtaining a regular decrease, degradation appeared intermittent. As a comparison standpoint, the degradation of nanoparticles in a solution mimicking the lysosomal environment of the cells (aqueous dispersion, pH 4, supplemented with 20 mM citrate serving as iron chelating agent) displayed a regular decrease (Fig. S4). After 6 days of real-time measurements, cell spheroids labeled with citrate were placed in the traditional incubator until day 21; they were then harvested and analyzed by TEM. Representative images **(Fig. 4G-I & S5)** show the presence of light grey dots in the endosomes and the cytoplasm, corresponding to iron stored in ferritin proteins typically observed upon the degradation of magnetic

nanoparticles, and confirming that degradation happens in a similar mode upon culture in the magnetic sensor.

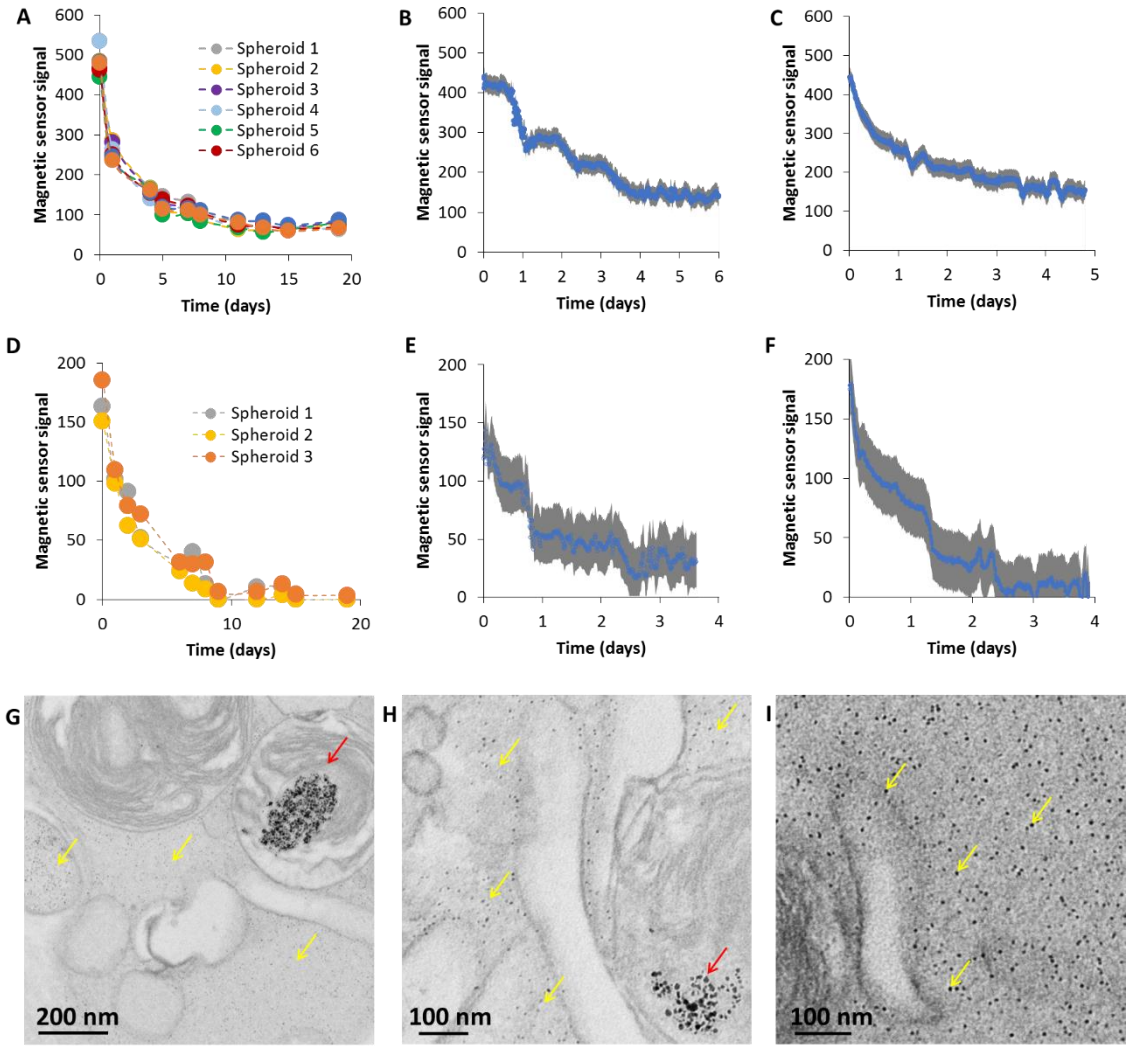

Figure 4: Magnetic sensor measurements allow long-term monitoring of the nanoparticles' biodegradation in operando on living cell spheroids. A-F) Magnetism of cell spheroids is analyzed using the magnetic sensor, either every few days for a few minutes with the samples being cultured in a standard incubator for the remaining time (A,C) or in real-time with data are obtained every 0.5 seconds for up to 6 continuous days and averaged every 10 minutes (B,D-F) (the grey area represents the measurement variations coming from the device). The cells are labeled with magnetic nanoparticles either coated with citrate (A,B,C) or PEG (D,E,F). G-I) TEM images taken upon 6 days of real-time recordings followed by traditional culture in an incubator for 15 days display the appearance of small grey dots (around 6 nm in diameter) in the endosomes and the cytoplasm of the cells, typical appearance of ferritin proteins loaded with iron released from the degradation of magnetic nanoparticles. Red arrows:

intact nanoparticles, yellow arrows: ferritin proteins.

Next step was to investigate any potential impact on stem cell functions (spheroid formation and differentiation capacity) of the real-time in situ continuous degradation monitoring inside the magnetic sensor. The chondrogenesis differentiation was investigated, as it is the one differentiation possible in the 3D spheroid geometry, and also because it is the differentiation which is the first to be impacted by environmental changes, such as exposure to nanoparticles. First, images of the spheroids over time showed their progressive development as a cohesive 3D structure along and upon continuous recordings, suggesting spheroid formation and contractility indicative of functional cell-cell adhesions **(Fig. 5A)**. Histological staining was then performed as an indicator of successful chondrogenesis through the production of proteoglycans. **Fig. 5B** evidences Safranin O staining for the samples cultured in the magnetic sensor at the same level than for those cultured in the traditional incubator. TEM observations at day 21 similarly evidenced synthesis of extracellular matrix components in both the spheroids cultured in the magnetic sensor **(Fig. 5C & S5)** as well as in the ones kept in the incubator **(Fig. 5D)**. Finally, gene expression of extracellular matrix components (aggregan, collagen type X, cartilage oligomeric matrix protein, transcription factor sox 9) specifically expressed during stem cell chondrogenic differentiation was assessed after 14 and 21 days of spheroid maturation. It displayed similar levels for the samples that were cultured in the magnetic sensor and for the ones remaining in the traditional incubator **(Fig. 5E)**.

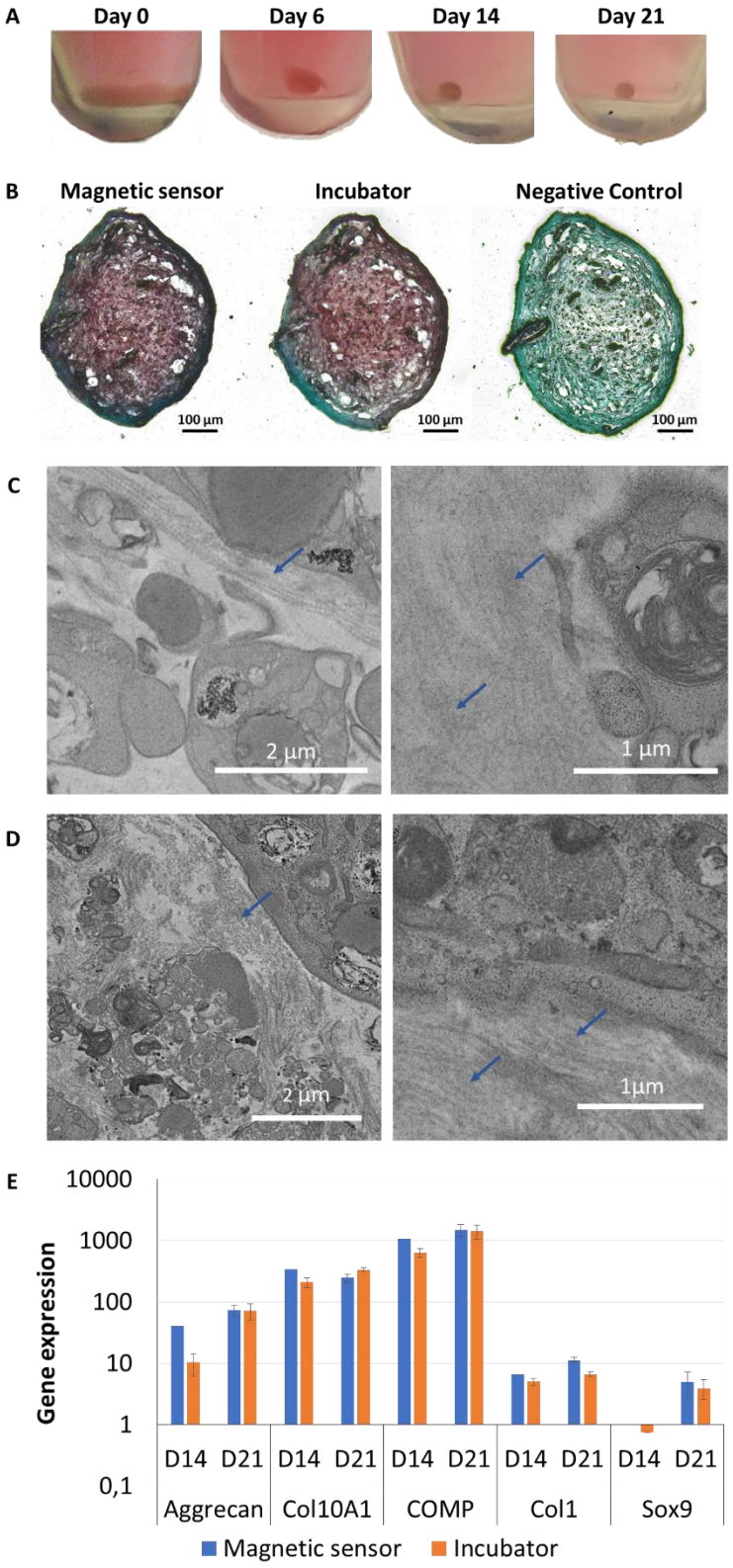

Figure 5: The cell spheroids remain viable along the real-time measurements using the magnetic sensor. A) Representative photographs taken upon centrifugation of the cells at day 0 and after 6 days of culture and continuous magnetometry measurements in the magnetic sensor show that the cells formed a cohesive 3D cell spheroid, similar structure to the one

obtained traditionally when cultured in an incubator. These spheroids are then cultured for 15 additional days in a traditional incubator (until day 21) and harvested for histology, PCR, and TEM analyses. B) Representative histological images of aggregates fixed at day 21 and stained with Safranin O reveal the presence of extracellular matrix components (glycosaminoglycans) in the aggregates cultured in the sensor under continuous magnetometry measurements (magnetic sensor condition) as well as in the ones cultured in the traditional incubator only (incubator condition). For both these conditions, the aggregates are stimulated with growth factors to initiate ECM formation, while the negative control was cultured in the incubator and without growth factor. C,D) Representative TEM images of samples cultured in the magnetic sensor (C) and in the incubator (D), after 21 days of culture with growth factors, show the formation of extracellular matrix (blue arrows) for both. E) Gene expression of extracellular matrix components at days 14 and 21 display similar gene expression for the cell spheroids in the magnetic sensor or in the incubator.

3. Discussion

There is undeniable potential for magnetic nanoparticles in biomedical applications [49]; however, the question of their fate once within the organism is not fully resolved yet. Studies performed *in vivo* demonstrated that injected nanoparticles are progressively degraded, join the iron pool, and integrate the iron metabolism [28,29,31,32,50]. More recently, quantitative measurements have been performed *in vitro* on a given pool of cells [33–35]. In this case, contrarily to the *in vivo* experiments, the entire pool of injected nanoparticles is followed on the long-term as no nanoparticle can circulate away from the system. The progressive degradation of nanoparticles within stem cells was demonstrated and reached up to 90% degradation over the course of a month [33]. It shed light on the transformations of nanoparticles within the cells; however, the integrity of the nanoparticles was tracked via their original magnetic properties that allow them to be monitored at a distance using magnetometry measurements; and these measures are performed on large-scale machines with limited accessibility, and impossible on living cells. As such, numerous discrete samples needed to be fixed for each data point resulting in data points at every few days only, and never on the exact same cell samples.

Herein, we introduce the use of a small, bench-top size, magnetic sensor for performing such assessments. This device provides a signal proportional to the magnetism of samples and was initially developed for immunoassays, using probes based on magnetic nanoparticles [48,51]. It has further been expanded to study the synthesis and functionalization of magnetic nanoparticles [52,53] and the internalization of nanoparticles in cells [54–56]. It also allowed

the non-invasive monitoring of nanoparticles *in vivo*; either by assessing their blood half-life in the tail veins of mice [57] or by non-invasive monitoring of their long-term distribution in various organs upon intra-arterial injection [58]. In the present study, the magnetic sensor serves as an innovative tool to assess the transformations of the nanoparticles *in vitro*, in a tissue model based on stem cells [33–35]. Briefly, stem cells are labeled with magnetic nanoparticles, centrifuged, and kept in culture such as they form a 3D cohesive tissue in the shape of a spheroid. This tissue model is advantageous as the culture parameters prevent cell proliferation, and the tissue formed is easy to manipulate and to keep in culture for months. Moreover, stem cells are a cell-source of choice for regenerative medicine applications and a full comprehension of the intracellular fate of nanoparticles is required for transitioning to the clinic. Also, stem cells provide an intracellular environment containing a large range of biomolecules including, among others, proteins related to iron metabolism and responsible for the assimilation of magnetic nanoparticles in the biological environment.

Results first demonstrate that the magnetic sensor is a relevant approach for the follow-up of the intracellular integrity of nanoparticles. Data obtained on punctual samples show the progressive degradation of the nanoparticles *in cellulo*, similarly to observations obtained with conventional magnetometry approaches, in agreement with previous works [33–35]. When compared to the VSM technique, a strong correlation is observed ($R^2 > 0.99$) between both measurements and the signal acquired with the magnetic sensor can then be converted in a magnetic moment (expressed in emu). It has to be noted that this correlation should be achieved for each nanoparticle type, as the signal of the magnetic sensor depends on each nanoparticle system [59]. Interestingly, the correlation between the magnetic sensor and the VSM measurements remains unchanged even upon degradation of the nanoparticles. It means that only nanoparticles in the size range of the internalized ones (9 nm) are measured, indicating an all-or-nothing degradation of the nanoparticles (the nanoparticles are either intact or fully degraded).

Additionally, and quite remarkably, the magnetic sensor allowed real-time follow-up of the magnetism of living cell spheroids over days, delineating precise variations in the biotransformation of the nanoparticles. This real-time degradation observed in the cell spheroid signal is much more fluctuated than the ones of the same nanoparticles in an aqueous medium at pH 4.5 with iron chelating agent (citrate), often used as lysosomal-like medium [60,61], where the magnetism decrease is regular. The more irregular degradation process is probably, and logically, linked to biological processes.

Remarkably, the cell spheroids subjected to continuous magnetic sensor measurements

remained totally functional, opening up to the real-time tracking of magnetic nanoparticles in tissues, important for some applications where the diagnostic and therapeutic potential of the nanoparticles in the long-term depend on their stability in the biological environment. The degradation of the nanoparticles could for example lead to a loss of signal in MRI imaging, an issue if the goal is to track implanted cells or grafts over a long period of time [62,63]. Moreover, the remote control of cells' spatial arrangements would also be reduced thus impacting *in vivo* targeting abilities and the magnetic development of 3D tissue constructs.

To conclude, the magnetic sensor is a small bench-top machine that can be easily set into a laboratory and used for a fast screen of cell labeling efficiency and for the *in situ* follow-up of time dependent nanoparticles' integrity, both on living cells.

Acknowledgments

This work was supported by the European Union (ERC-2014-CoG project MaTissE #648779). The authors would like to acknowledge the CNanoMat physico-chemical characterizations platform of University Paris 13, and Nicolas Chevalier for his help in controlling the CO_2 level in the home-made incubator associated to the magnetic sensor.

References

[1] Wei, H.; Bruns, O.T.; Kaul, M.G.; Hansen, E.C.; Barch, M.; Wiśniowska, A.; Chen, O.; Chen, Y.; Li, N.; Okada, S.; Cordero, J.M.; Heine, M.; Farrar, C.T.; Montana, D.M.; Adam, G.; Ittrich, H.; Jasanoff, A.; Nielsen, P.; Bawendi, M.G. Exceedingly Small Iron Oxide Nanoparticles as Positive MRI Contrast Agents. *Proc. Natl. Acad. Sci. U. S. A.*, **2017**, *114*, 2325–2330.

[2] Hachani, R.; Lowdell, M.; Birchall, M.; Hervault, A.; Mertz, D.; Begin-Colin, S.; Thanh, N.T.K. Polyol Synthesis, Functionalisation, and Biocompatibility Studies of Superparamagnetic Iron Oxide Nanoparticles as Potential MRI Contrast Agents. *Nanoscale*, **2016**, *8*, 3278–3287.

[3] Blanco-Andujar, C.; Walter, A.; Cotin, G.; Bordeianu, C.; Mertz, D.; Felder-Flesch, D.; Begin-Colin, S. Design of Iron Oxide-Based Nanoparticles for MRI and Magnetic Hyperthermia. *Nanomed.*, **2016**, *11*, 1889–1910.

[4] Cotin, G.; Blanco-Andujar, C.; Nguyen, D.-V.; Affolter, C.; Boutry, S.; Boos, A.; Ronot, P.; Uring-Lambert, B.; Choquet, P.; Zorn, P.E.; Mertz, D.; Laurent, S.; Muller, R.N.; Meyer, F.; Felder Flesch, D.; Begin-Colin, S. Dendron Based Antifouling, MRI and Magnetic Hyperthermia Properties of Different Shaped Iron Oxide Nanoparticles. *Nanotechnology*, **2019**, *30*, 374002.

[5] Cortajarena, A.L.; Ortega, D.; Ocampo, S.M.; Gonzalez-García, A.; Couleaud, P.; Miranda, R.; Belda-Iniesta, C.; Ayuso-Sacido, A. Engineering Iron Oxide Nanoparticles for Clinical Settings. *Nanobiomedicine*, **2014**, *1*, 2.

[6] Johannsen, M.; Thiesen, B.; Wust, P.; Jordan, A. Magnetic Nanoparticle Hyperthermia for Prostate Cancer. *Int. J. Hyperthermia*, **2010**, *26*, 790–795.

[7] Blanco-Andujar, C.; Teran, F.J.; Ortega, D. Chapter 8 - Current Outlook and Perspectives on Nanoparticle-Mediated Magnetic Hyperthermia. In *Iron Oxide Nanoparticles for Biomedical Applications*; Mahmoudi, M.; Laurent, S., Eds.; Metal Oxides; Elsevier, **2018**; pp. 197–245.

[8] Maier-Hauff, K.; Ulrich, F.; Nestler, D.; Niehoff, H.; Wust, P.; Thiesen, B.; Orawa, H.; Budach, V.; Jordan, A. Efficacy and Safety of Intratumoral Thermotherapy Using Magnetic Iron-Oxide Nanoparticles Combined with External Beam Radiotherapy on Patients with Recurrent Glioblastoma Multiforme. *J. Neurooncol.*, **2011**, *103*, 317–324.

[9] Espinosa, A.; Kolosnjaj-Tabi, J.; Abou-Hassan, A.; Sangnier, A.P.; Curcio, A.; Silva, A.K.A.; Corato,

R.D.; Neveu, S.; Pellegrino, T.; Liz-Marzán, L.M.; Wilhelm, C. Magnetic (Hyper)Thermia or Photothermia? Progressive Comparison of Iron Oxide and Gold Nanoparticles Heating in Water, in Cells, and In Vivo. *Adv. Funct. Mater.*, **2018**, *28*, 1803660.

[10] Kakwere, H.; Leal, M.P.; Materia, M.E.; Curcio, A.; Guardia, P.; Niculaes, D.; Marotta, R.; Falqui, A.; Pellegrino, T. Functionalization of Strongly Interacting Magnetic Nanocubes with (Thermo)Responsive Coating and Their Application in Hyperthermia and Heat-Triggered Drug Delivery. *ACS Appl. Mater. Interfaces*, **2015**, *7*, 10132–10145.

[11] Sandre, O.; Genevois, C.; Garaio, E.; Adumeau, L.; Mornet, S.; Couillaud, F. In Vivo Imaging of Local Gene Expression Induced by Magnetic Hyperthermia. *Genes*, **2017**, *8*.

[12] Mai, B.T.; Balakrishnan, P.B.; Barthel, M.J.; Piccardi, F.; Niculaes, D.; Marinaro, F.; Fernandes, S.; Curcio, A.; Kakwere, H.; Autret, G.; Cingolani, R.; Gazeau, F.; Pellegrino, T. Thermoresponsive Iron Oxide Nanocubes for an Effective Clinical Translation of Magnetic Hyperthermia and Heat-Mediated Chemotherapy. *ACS Appl. Mater. Interfaces*, **2019**, *11*, 5727–5739.

[13] Blanco-Andujar, C.; Ortega, D.; Southern, P.; Pankhurst, Q.A.; Thanh, N.T.K. High Performance Multi-Core Iron Oxide Nanoparticles for Magnetic Hyperthermia: Microwave Synthesis, and the Role of Core-to-Core Interactions. *Nanoscale*, **2015**, *7*, 1768–1775.

[14] Asensio, J.M.; Marbaix, J.; Mille, N.; Lacroix, L.-M.; Soulantica, K.; Fazzini, P.-F.; Carrey, J.; Chaudret, B. To Heat or Not to Heat: A Study of the Performances of Iron Carbide Nanoparticles in Magnetic Heating. *Nanoscale*, **2019**, *11*, 5402–5411.

[15] Hallali, N.; Clerc, P.; Fourmy, D.; Gigoux, V.; Carrey, J. Influence on Cell Death of High Frequency Motion of Magnetic Nanoparticles during Magnetic Hyperthermia Experiments. *Appl. Phys. Lett.*, **2016**, *109*, 032402.

[16] Plan Sangnier, A.; Preveral, S.; Curcio, A.; K. A. Silva, A.; Lefèvre, C.T.; Pignol, D.; Lalatonne, Y.; Wilhelm, C. Targeted Thermal Therapy with Genetically Engineered Magnetite Magnetosomes@RGD: Photothermia Is Far More Efficient than Magnetic Hyperthermia. *J. Controlled Release*, **2018**, *279*, 271–281.

[17] Chu, M.; Shao, Y.; Peng, J.; Dai, X.; Li, H.; Wu, Q.; Shi, D. Near-Infrared Laser Light Mediated Cancer Therapy by Photothermal Effect of Fe3O4 Magnetic Nanoparticles. *Biomaterials*, **2013**, *34*, 4078–4088.

[18] Zhou, Z.; Sun, Y.; Shen, J.; Wei, J.; Yu, C.; Kong, B.; Liu, W.; Yang, H.; Yang, S.; Wang, W. Iron/Iron Oxide Core/Shell Nanoparticles for Magnetic Targeting MRI and near-Infrared Photothermal Therapy. *Biomaterials*, **2014**, *35*, 7470–7478.

[19] Shen, S.; Wang, S.; Zheng, R.; Zhu, X.; Jiang, X.; Fu, D.; Yang, W. Magnetic Nanoparticle Clusters for Photothermal Therapy with Near-Infrared Irradiation. *Biomaterials*, **2015**, *39*, 67–74.

[20] Ye, D.; Li, Y.; Gu, N. Magnetic Labeling of Natural Lipid Encapsulations with Iron-Based Nanoparticles. *Nano Res.*, **2018**, *11*, 2970–2991.

[21] Ulbrich, K.; Holá, K.; Šubr, V.; Bakandritsos, A.; Tuček, J.; Zbořil, R. Targeted Drug Delivery with Polymers and Magnetic Nanoparticles: Covalent and Noncovalent Approaches, Release Control, and Clinical Studies. *Chem. Rev.*, **2016**, *116*, 5338–5431.

[22] Carregal-Romero, S.; Guardia, P.; Yu, X.; Hartmann, R.; Pellegrino, T.; Parak, W.J. Magnetically Triggered Release of Molecular Cargo from Iron Oxide Nanoparticle Loaded Microcapsules. *Nanoscale*, **2014**, *7*, 570–576.

[23] Mertz, D.; Sandre, O.; Bégin-Colin, S. Drug Releasing Nanoplatforms Activated by Alternating Magnetic Fields. *Biochim. Biophys. Acta BBA - Gen. Subj.*, **2017**, *1861*, 1617–1641.

[24] Adedoyin, A.A.; Ekenseair, A.K. Biomedical Applications of Magneto-Responsive Scaffolds. *Nano Res.*, **2018**, *11*, 5049–5064.

[25] Souza, G.R.; Molina, J.R.; Raphael, R.M.; Ozawa, M.G.; Stark, D.J.; Levin, C.S.; Bronk, L.F.; Ananta, J.S.; Mandelin, J.; Georgescu, M.-M.; Bankson, J.A.; Gelovani, J.G.; Killian, T.C.; Arap, W.; Pasqualini, R. Three-Dimensional Tissue Culture Based on Magnetic Cell Levitation. *Nat. Nanotechnol.*, **2010**, *5*, 291–296.

[26] Mattix, B.; Olsen, T.R.; Gu, Y.; Casco, M.; Herbst, A.; Simionescu, D.T.; Visconti, R.P.; Kornev, K.G.; Alexis, F. Biological Magnetic Cellular Spheroids as Building Blocks for Tissue Engineering. *Acta Biomater.*, **2014**, *10*, 623–629.

[27] Hachani, R.; Lowdell, M.; Birchall, M.; Thanh, N.T.K. Tracking Stem Cells in Tissue-Engineered Organs Using Magnetic Nanoparticles. *Nanoscale*, **2013**, *5*, 11362–11373.

[28] Pham, B.T.T.; Colvin, E.K.; Pham, N.T.H.; Kim, B.J.; Fuller, E.S.; Moon, E.A.; Barbey, R.; Yuen, S.; Rickman, B.H.; Bryce, N.S.; Bickley, S.; Tanudji, M.; Jones, S.K.; Howell, V.M.; Hawkett, B.S. Biodistribution and Clearance of Stable Superparamagnetic Maghemite Iron Oxide Nanoparticles in Mice Following Intraperitoneal Administration. *Int. J. Mol. Sci.*, **2018**, *19*.

[29] Bargheer, D.; Giemsa, A.; Freund, B.; Heine, M.; Waurisch, C.; Stachowski, G.M.; Hickey, S.G.; Eychmüller, A.; Heeren, J.; Nielsen, P. The Distribution and Degradation of Radiolabeled

Superparamagnetic Iron Oxide Nanoparticles and Quantum Dots in Mice. *Beilstein J. Nanotechnol.*, **2015**, *6*, 111–123.

[30] Freund, B.; Tromsdorf, U.I.; Bruns, O.T.; Heine, M.; Giemsa, A.; Bartelt, A.; Salmen, S.C.; Raabe, N.; Heeren, J.; Ittrich, H.; Reimer, R.; Hohenberg, H.; Schumacher, U.; Weller, H.; Nielsen, P. A Simple and Widely Applicable Method to 59Fe-Radiolabel Monodisperse Superparamagnetic Iron Oxide Nanoparticles for in Vivo Quantification Studies. *ACS Nano*, **2012**, *6*, 7318–7325.

[31] Singh, S.P.; Rahman, M.F.; Murty, U.S.N.; Mahboob, M.; Grover, P. Comparative Study of Genotoxicity and Tissue Distribution of Nano and Micron Sized Iron Oxide in Rats after Acute Oral Treatment. *Toxicol. Appl. Pharmacol.*, **2013**, *266*, 56–66.

[32] Gu, L.; Fang, R.H.; Sailor, M.J.; Park, J.-H. In Vivo Clearance and Toxicity of Monodisperse Iron Oxide Nanocrystals. *ACS Nano*, **2012**, *6*, 4947–4954.

[33] Mazuel, F.; Espinosa, A.; Luciani, N.; Reffay, M.; Le Borgne, R.; Motte, L.; Desboeufs, K.; Michel, A.; Pellegrino, T.; Lalatonne, Y.; Wilhelm, C. Massive Intracellular Biodegradation of Iron Oxide Nanoparticles Evidenced Magnetically at Single-Endosome and Tissue Levels. *ACS Nano*, **2016**, *10*, 7627–7638.

[34] Sangnier, A.P.; Walle, A.V. de; Curcio, A.; Borgne, R.L.; Motte, L.; Lalatonne, Y.; Wilhelm, C. Impact of Magnetic Nanoparticle Surface Coating on Their Long-Term Intracellular Biodegradation in Stem Cells. *Nanoscale*, **2019**.

[35] Van de Walle, A.; Plan Sangnier, A.; Abou-Hassan, A.; Curcio, A.; Hémadi, M.; Menguy, N.; Lalatonne, Y.; Luciani, N.; Wilhelm, C. Biosynthesis of Magnetic Nanoparticles from Nano-Degradation Products Revealed in Human Stem Cells. *Proc. Natl. Acad. Sci. U. S. A.*, **2019**.

[36] Hemery, G.; Garanger, E.; Lecommandoux, S.; Wong, A.D.; Gillies, E.R.; Pedrono, B.; Bayle, T.; Jacob, D.; Sandre, O. Thermosensitive Polymer-Grafted Iron Oxide Nanoparticles Studied Byin Situdynamic Light Backscattering under Magnetic Hyperthermia. *J. Phys. Appl. Phys.*, **2015**, *48*, 494001.

[37] Wang, L.; Wang, Z.; Li, X.; Zhang, Y.; Yin, M.; Li, J.; Song, H.; Shi, J.; Ling, D.; Wang, L.; Chen, N.; Fan, C. Deciphering Active Biocompatibility of Iron Oxide Nanoparticles from Their Intrinsic Antagonism. *Nano Res.*, **2018**, *11*, 2746–2755.

[38] Wilhelm, C.; Gazeau, F. Universal Cell Labelling with Anionic Magnetic Nanoparticles. *Biomaterials*, **2008**, *29*, 3161–3174.

[39] Negi, H.; Takeuchi, S.; Kamei, N.; Yanada, S.; Adachi, N.; Ochi, M. Safety and Quality of Magnetically Labeled Human Mesenchymal Stem Cells for Cartilage Repair. *Tissue Eng. Part C Methods*, **2019**.

[40] Van de Walle, A.; Faissal, W.; Wilhelm, C.; Luciani, N. Role of Growth Factors and Oxygen to Limit Hypertrophy and Impact of High Magnetic Nanoparticles Dose during Stem Cell Chondrogenesis. *Comput. Struct. Biotechnol. J.*, **2018**, *16*, 532–542.

[41] Chang, Y.-K.; Liu, Y.-P.; Ho, J.H.; Hsu, S.-C.; Lee, O.K. Amine-Surface-Modified Superparamagnetic Iron Oxide Nanoparticles Interfere with Differentiation of Human Mesenchymal Stem Cells. *J. Orthop. Res. Off. Publ. Orthop. Res. Soc.*, **2012**, *30*, 1499–1506.

[42] Chen, Y.-C.; Hsiao, J.-K.; Liu, H.-M.; Lai, I.-Y.; Yao, M.; Hsu, S.-C.; Ko, B.-S.; Chen, Y.-C.; Yang, C.-S.; Huang, D.-M. The Inhibitory Effect of Superparamagnetic Iron Oxide Nanoparticle (Ferucarbotran) on Osteogenic Differentiation and Its Signaling Mechanism in Human Mesenchymal Stem Cells. *Toxicol. Appl. Pharmacol.*, **2010**, *245*, 272–279.

[43] Huang, D.-M.; Hsiao, J.-K.; Chen, Y.-C.; Chien, L.-Y.; Yao, M.; Chen, Y.-K.; Ko, B.-S.; Hsu, S.-C.; Tai, L.-A.; Cheng, H.-Y.; Wang, S.-W.; Yang, C.-S.; Chen, Y.-C. The Promotion of Human Mesenchymal Stem Cell Proliferation by Superparamagnetic Iron Oxide Nanoparticles. *Biomaterials*, **2009**, *30*, 3645–3651.

[44] Roeder, E.; Henrionnet, C.; Goebel, J.C.; Gambier, N.; Beuf, O.; Grenier, D.; Chen, B.; Vuissoz, P.-A.; Gillet, P.; Pinzano, A. Dose-Response of Superparamagnetic Iron Oxide Labeling on Mesenchymal Stem Cells Chondrogenic Differentiation: A Multi-Scale in Vitro Study. *PloS One*, **2014**, *9*, e98451.

[45] Nikitin, P.I.; Vetoshko, P.M.; Ksenevich, T.I. New Type of Biosensor Based on Magnetic Nanoparticle Detection. *J. Magn. Magn. Mater.*, **2007**, *311*, 445–449.

[46] Lenglet, L.; Motte, L. Chapter 8 - Neel Effect: Exploiting the Nonlinear Behavior of Superparamagnetic Nanoparticles for Applications in Life Sciences up to Electrical Engineering. In *Novel Magnetic Nanostructures*; Domracheva, N.; Caporali, M.; Rentschler, E., Eds.; Advanced Nanomaterials; Elsevier, **2018**; pp. 247–265.

[47] Richard, S.; Eder, V.; Caputo, G.; Journé, C.; Ou, P.; Bolley, J.; Louedec, L.; Guenin, E.; Motte, L.; Pinna, N.; Lalatonne, Y. USPIO Size Control through Microwave Nonaqueous Sol-Gel Method for Neoangiogenesis T2 MRI Contrast Agent. *Nanomed.*, **2016**, *11*, 2769–2779.

[48] Motte, L.; Benyettou, F.; Beaucorps, C. de; Lecouvey, M.; Milesovic, I.; Lalatonne, Y. Multimodal Superparamagnetic Nanoplatform for Clinical Applications: Immunoassays, Imaging & Therapy. *Faraday Discuss.*, **2013**, *149*, 211–225.

[49] Assa, F.; Jafarizadeh-Malmiri, H.; Ajamein, H.; Anarjan, N.; Vaghari, H.; Sayyar, Z.; Berenjian, A. A Biotechnological Perspective on the Application of Iron Oxide Nanoparticles. *Nano Res.*, **2016**, *9*, 2203–2225.

[50] Tamion, A.; Hillenkamp, M.; Hillion, A.; Maraloiu, V.A.; Vlaicu, I.D.; Stefan, M.; Ghica, D.; Rositi, H.; Chauveau, F.; Blanchin, M.-G.; Wiart, M.; Dupuis, V. Ferritin Surplus in Mouse Spleen 14 Months after Intravenous Injection of Iron Oxide Nanoparticles at Clinical Dose. *Nano Res.*, **2016**, *9*, 2398–2410.

[51] Nikitin, P.I.; Vetoshko, P.M.; Ksenevich, T.I. Magnetic Immunoassays https://www.ingentaconnect.com/content/asp/senlet/2007/00000005/00000001/art00077 (accessed Aug 27, 2019).

[52] Guénin, E.; Lalatonne, Y.; Bolley, J.; Milosevic, I.; Platas-Iglesias, C.; Motte, L. Catechol versus Bisphosphonate Ligand Exchange at the Surface of Iron Oxide Nanoparticles: Towards Multi-Functionalization. *J. Nanoparticle Res.*, **2014**, *16*, 2596.

[53] Milosevic, I.; Warmont, F.; Lalatonne, Y.; Motte, L. Magnetic Metrology for Iron Oxide Nanoparticle Scaled-up Synthesis. *RSC Adv.*, **2014**, *4*, 49086–49089.

[54] Geinguenaud, F.; Souissi, I.; Fagard, R.; Motte, L.; Lalatonne, Y. Electrostatic Assembly of a DNA Superparamagnetic Nano-Tool for Simultaneous Intracellular Delivery and in Situ Monitoring. *Nanomedicine Nanotechnol. Biol. Med.*, **2012**, *8*, 1106–1115.

[55] Geinguenaud, F.; Souissi, I.; Fagard, R.; Lalatonne, Y.; Motte, L. Easily Controlled Grafting of Oligonucleotides on ΓFe2O3 Nanoparticles: Physicochemical Characterization of DNA Organization and Biological Activity Studies. *J. Phys. Chem. B*, **2014**, *118*, 1535–1544.

[56] Benyettou, F.; Fahs, H.; Elkharrag, R.; Bilbeisi, R.A.; Asma, B.; Rezgui, R.; Motte, L.; Magzoub, M.; Brandel, J.; Olsen, J.-C.; Piano, F.; Gunsalus, K.C.; Platas-Iglesias, C.; Trabolsi, A. Selective Growth Inhibition of Cancer Cells with Doxorubicin-Loaded CB[7]-Modified Iron-Oxide Nanoparticles. *RSC Adv.*, **2017**, *7*, 23827–23834.

[57] Nikitin, M.P.; Vetoshko, P.M.; Brusentsov, N.A.; Nikitin, P.I. Highly Sensitive Room-Temperature Method of Non-Invasive in Vivo Detection of Magnetic Nanoparticles. *J. Magn. Magn. Mater.*, **2009**, *321*, 1658–1661.

[58] Nikitin, M.; Yuriev, M.; Brusentsov, N.; Vetoshko, P.; Nikitin, P. Non-Invasive in Vivo Mapping and Long-Term Monitoring of Magnetic Nanoparticles in Different Organs of Animals. *AIP Conf. Proc.*, **2010**, *1311*, 452–457.

[59] de Montferrand, C.; Hu, L.; Milosevic, I.; Russier, V.; Bonnin, D.; Motte, L.; Brioude, A.; Lalatonne, Y. Iron Oxide Nanoparticles with Sizes, Shapes and Compositions Resulting in Different Magnetization Signatures as Potential Labels for Multiparametric Detection. *Acta Biomater.*, **2013**, *9*, 6150–6157.

[60] Arbab, A.S.; Wilson, L.B.; Ashari, P.; Jordan, E.K.; Lewis, B.K.; Frank, J.A. A Model of Lysosomal Metabolism of Dextran Coated Superparamagnetic Iron Oxide (SPIO) Nanoparticles: Implications for Cellular Magnetic Resonance Imaging. *NMR Biomed.*, **2005**, *18*, 383–389.

[61] Gutiérrez, L.; Romero, S.; da Silva, G.B.; Costo, R.; Vargas, M.D.; Ronconi, C.M.; Serna, C.J.; Veintemillas-Verdaguer, S.; Del Puerto Morales, M. Degradation of Magnetic Nanoparticles Mimicking Lysosomal Conditions Followed by AC Susceptibility. *Biomed. Tech. (Berl)*, **2015**, *60*, 417–425.

[62] Soenen, S.J.H.; Himmelreich, U.; Nuytten, N.; Pisanic, T.R.; Ferrari, A.; De Cuyper, M. Intracellular Nanoparticle Coating Stability Determines Nanoparticle Diagnostics Efficacy and Cell Functionality. *Small Weinh. Bergstr. Ger.*, **2010**, *6*, 2136–2145.

[63] Garcés, V.; Rodríguez-Nogales, A.; González, A.; Gálvez, N.; Rodríguez-Cabezas, M.E.; García-Martin, M.L.; Gutiérrez, L.; Rondón, D.; Olivares, M.; Gálvez, J.; Dominguez-Vera, J.M. Bacteria-Carried Iron Oxide Nanoparticles for Treatment of Anemia. *Bioconjug. Chem.*, **2018**, *29*, 1785–1791.